Evaluating the Potential for Retrieving Aerosol Optical Depth over Land from AVHRR Pathfinder Atmosphere Data

Kenneth R. Knapp

Cooperative Institute for Research in the Atmosphere, Camp Springs, Maryland

Larry L. Stowe

NOAA/NESDIS/Office of Research and Applications, Camp Springs, Maryland

ABSTRACT

In spite of numerous studies on the remote sensing of aerosols from satellites, the magnitude of aerosol climate forcing remains uncertain. However, data from the Advanced Very High Resolution Radiometer (AVHRR) Pathfinder-Atmosphere (PATMOS) dataset—a statistical reduction of more than 19 yr of AVHRR data (1981–2000)—could provide nearly 20 yr of aerosol history. PATMOS data have a daily 110×110 km² equal-area grid that contains means and standard deviations of AVHRR observations within each grid cell. This research is a first step toward understanding aerosols over land with PATMOS data. Herein, the aerosol optical depth is retrieved over land at numerous Aerosol Robotic Network (AERONET) sites around the globe using PATMOS cloud-free reflectances. First, the surface bidirectional reflectance distribution function (BRDF) is retrieved using a lookup table created with a radiative transfer model and the Rahman BRDF. Aerosol optical depths are then retrieved using the retrieved BRDF parameters and the PATMOS reflectances assuming a globally constant aerosol model. This method is applied to locations with ground truth measurements, where comparisons show that the best retrievals are made by estimating the surface reflectance using observations grouped by month. Random errors (i.e., correlation coefficients and standard error of estimate) in this case are lower than those where the surface BRDF is allowed year-to-year variations. By grouping the comparison results by land cover type, it was found that less noise is expected over forested regions, with a significant potential for retrieval for 80% of all land surfaces. These results and analyses suggest that the PATMOS data can provide valuable information on aerosols over land.

1. Introduction

The Advanced Very High Resolution Radiometer (AVHRR) instrument has been used by numerous researchers to detect aerosol optical properties over the oceans (e.g., Stowe et al. 1997; Husar et al. 1997; Hindman et al. 1984). It is used by the National Oceanic and Atmospheric Administration (NOAA) to generate maps of aerosol optical depth τ operationally. In general, the ocean has a low, spectrally flat surface reflectance that is spatially uniform and whose bidirectional reflectance distribution function (BRDF) is well-characterized. These characteristics, along with the large portion of the earth covered by water, have made possible significant research on satellite aerosol remote sensing from AVHRR, and in some cases the ability of retrievals to estimate aerosol size (Higurashi et al. 2000; Mishchenko et al. 1999).

While algorithms have been developed for newer satellite instruments [e.g., the Sea-viewing Wide Field-of view Sensor (SeaWiFS; Wang et al. 2000) and the moderate resolution imaging spectroradiometer (MODIS; Tanré et al. 1997)], the AVHRR instrument provides a temporal coverage that the newest satellite sensors cannot provide for 20 yr. The current version of the AVHRR was first launched in an afternoon orbit on *NOAA-7* in 1981. Since then, AVHRR sensors have flown on three more afternoon NOAA satellites (preferred over morning orbits due to better solar illumination) with the only gap in coverage from September 1994 to February 1995 when the *NOAA-11* AVHRR failed. This global afternoon coverage of nearly 20 yr includes two major volcanic eruptions (El Chichón in 1982 and Mt. Pinatubo in 1991) and provides a significant opportunity to understand the spatial and temporal distribution of aerosols over nearly two decades. Research toward this end has begun (e.g., Husar et al. 1997; Stowe et al. 1997; Stowe et al. 2002; Higurashi et al. 2000) and is ongoing through the NASA-funded Global Aerosol Climatology Project. However, the majority of the AVHRR remote

Corresponding author address: Kenneth R. Knapp, NOAA/NESDIS/ORA/CIRA, Room 711, 5200 Auth Rd., Camp Springs, MD 20746-4304.
E-mail: kenknapp@noaa.gov

© 2002 American Meteorological Society

sensing research is directed toward retrieving the most accurate aerosol information over ocean. The purpose of this research effort is to show that the AVHRR instrument can also provide aerosol information over some land surfaces, which may be incorporated into an aerosol climatology.

The bulk of the AVHRR remote sensing over land (at visible wavelengths) has concentrated on the retrieval of surface information, specifically the normalized difference vegetation index (NDVI) and albedo. The NDVI was developed using the AVHRR and has been used by many to characterize the global land cover (e.g., DeFries and Townshend 1994). It has also been linked to vegetation characteristics such as leaf area index (Schuessel et al. 1994). Studies have investigated methods to correct the NDVI and other surface features for the atmospheric effects of gaseous absorption and aerosol extinction (e.g., Rahman and Dedieu 1994; Mitchell and O'Brien 1993; Justice et al. 1991). Even the effect of NOAA satellite orbital drift on NDVI has been investigated (Privette et al. 1995; Gutman 1999). Generally, NDVI is used to determine characteristics of the land cover vegetation while the BRDF and albedo retrievals are used to understand the radiative properties of the surface.

Surface albedo is the hemispherical average reflectance of a surface. It is required by weather and climate models to distribute solar radiation in the earth–atmosphere system. To calculate accurately, knowledge of the surface BRDF is required. The BRDF has been retrieved for regions of interest, such as the boreal forest (Deering et al. 1999; Li et al. 1996) and the Australian outback (O'Brien et al. 1998). It has also been retrieved globally by Csiszar and Gutman (1999) and Zhang et al. (1998)—both with global albedo distribution as the final objective. Albedo retrieval methods have also been developed using AVHRR data with the plan to transfer algorithms to the MODIS and multiangle imaging spectroradiometer instruments (Privette et al. 1997; Wanner et al. 1997).

Since research has shown that aerosol effects can be removed, then, in principle, aerosol optical properties (particularly optical depth) might also be retrieved. Yet, the advantages of retrieving aerosol over ocean are not available over land.

- Land surfaces generally have a higher surface reflectance than the oceans, so they provide less sensitivity to changes in aerosols.
- Models of the angular reflectance properties, described by the surface BRDF, are numerous and few have been applied globally. Also, the wavelength dependence of features ranges from bare surfaces, with weak spectral variation, to vegetated canopies with strong spectral variation.
- Land reflectance properties vary spatially and temporally on many scales. Spatial scales range from local changes due to urbanization to large-scale changes in

natural land cover, while temporal scales range from seasonal vegetative growth to daily changes (e.g., in soil reflectance after rain).

Therefore, few researchers have attempted to use AVHRR to sense aerosols over land. Regional studies have been performed in Tadhikistan (Fraser 1993) where retrievals of desert dust from full-resolution AVHRR data are found to have a 0.2 standard error of estimate. In another study on AVHRR remote sensing of aerosols over land, Fraser and Kaufman (1985) showed that the aerosol contribution to the top-of-the-atmosphere (TOA) reflectance decreases relative to the surface contribution as the surface reflectance increases. This allows for the retrieval of single-scatter albedo (ω_o) in addition to τ in regions with large gradients in surface reflectance (i.e., cf. Kaufman and Joseph 1982; Kaufman 1987). Further studies have used this technique, in addition to the ability to retrieve size estimates over oceans, to iteratively retrieve three properties of the aerosols (τ, ω_o, and effective radius) near coastlines (Kaufman et al. 1990). The structure of the land features also provides aerosol information because aerosols tend to decrease the contrast in an image (Holben et al. 1992). These studies, however, have been limited in scale and application and are thus difficult to incorporate into a global aerosol climatology. Therefore, this study will show how τ can be retrieved using a new AVHRR dataset, thereby making analysis possible for the full temporal (1981–2000) and spatial (global coverage) domain of the AVHRR data.

The Pathfinder-Atmosphere (PATMOS) dataset (Jacobowitz 1999; Stowe et al. 2002) is a statistical reduction of the global area coverage (GAC) AVHRR imagery to a 110×110 km² equal area grid. Cloud-free reflectances from PATMOS are used to characterize the land surface by retrieving parameters of a BRDF model with radiative transfer computations. The method is generic so it can be applied globally, but the present analysis is limited to sites with surface measurements of aerosol optical depth. The retrieved BRDF parameters allow the simulation of the expected TOA reflectances due to varying aerosol optical depths in the form of lookup tables (LUTs). These LUTs are then used to retrieve aerosol optical depths τ_P from the cloud-free observations, which are then compared to surface measurements of τ. These comparisons are then grouped by land cover class, since these comparisons suggest that retrieval accuracy depends on land class type. This may be due to the use of a simple global aerosol model or departures of the true BRDF from the model. Analysis also suggests that certain observation conditions (e.g., certain satellite viewing angles) could be selected to decrease the random error in future retrievals.

The next section describes the PATMOS data used to retrieve aerosol optical depth τ_P. The retrieval method is then presented in section 3, and section 4 evaluates
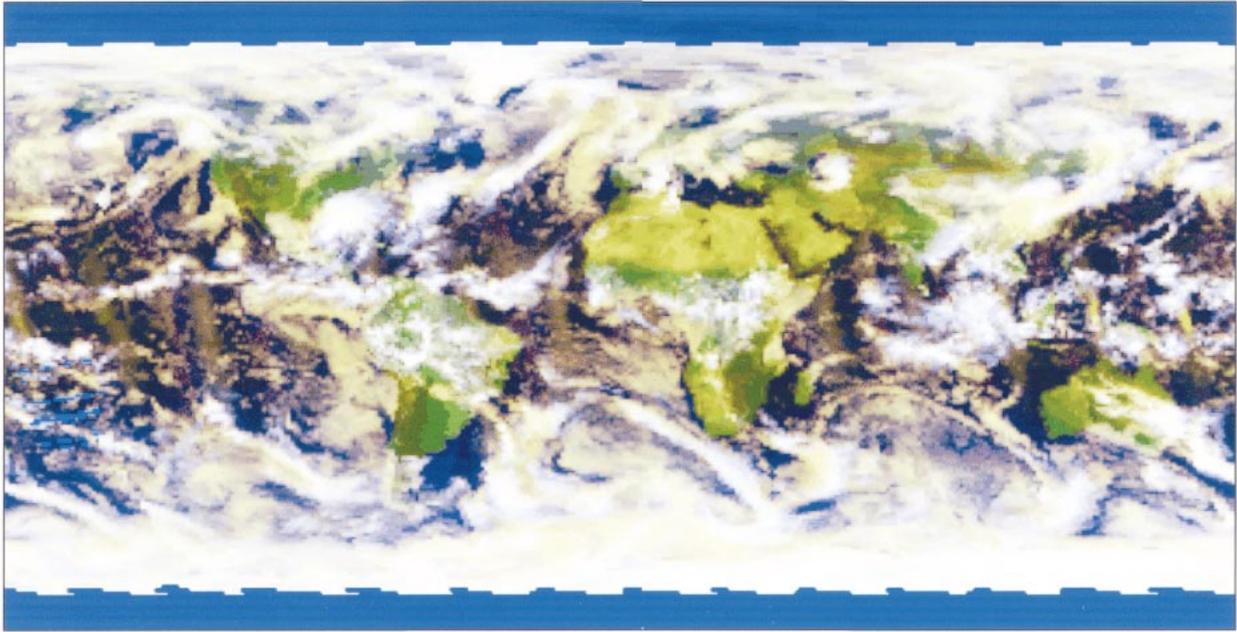
FIG. 1. False color image created from PATMOS all-sky reflectances and radiances using visible reflectance (channel 1, 0.63 μm) for red, near-infrared reflectance (channel 2, 0.83 μm) for green, and infrared radiances (channel 4, 10.8 μm) for blue. Visible features include synoptic-scale cloud fields and variation in the surface type (where deserts appear yellowish and vegetated areas are green).

the retrieval results using ground measurements of aerosol optical depth as ''truth.'' Finally, in section 5, conclusions are made in the context of the potential for a global aerosol climatology.

2. Dataset summary

The two primary sources of data used in this study are the PATMOS dataset, a subset of which provides cloud-free TOA reflectance observations, and aerosol optical depths from the Aerosol Robotic Network (AERONET; Holben et al. 1998). Also, a land cover classification from DeFries and Townshend (1994) is used in analyzing the retrieval results.

a. PATMOS data

The five-channel AVHRR-2 has flown nearly continuously on numerous NOAA satellites since 1981. This vast amount of data is condensed from terabytes to gigabytes and into a useable format in the PATMOS grid cell dataset. For each grid cell, radiance statistics are calculated for each AVHRR channel. An example of 1 day of PATMOS coverage is shown in Fig. 1. PATMOS data are more thoroughly described by S01.

The PATMOS daily-radiance dataset includes 71 parameters for each grid cell, 54 of which are directly derived from AVHRR pixel observations. Four GAC pixel-level scene identification categories are used to collect statistics (e.g., mean and std dev) for each channel: all-sky, cloud-free, aerosol-burden, and cloudy. The

parameters used in this study are the channel 1 (0.63 μm) reflectances (R_{sat}) for cloud-free (CF) and aerosol-burden (AB) pixels that have been normalized by earth–sun distance and corrected for known calibration drifts (Rao and Chen 1995). The CF reflectances are those pixels in a grid cell deemed cloud-free by the Clouds from AVHRR (CLAVR) algorithm (Stowe et al. 1999). The CLAVR algorithm uses spectral and spatial threshold tests to estimate cloud occurrence and works extremely well, except in high latitude winters. The AB reflectances are not estimates of aerosol properties but are the CF pixels in the darkest 30% of the channel-3 (3.7 μm) estimated reflectances over land. They are included in PATMOS in an attempt to limit the pixels to those with the most vegetation (i.e., the lowest reflectance at 3.7 μm). The AB reflectances are likely to be less cloud-contaminated, because the process is effectively adding another cloud screening criterion, and possibly less noisy, because they tend to come from similar portions of the grid cell. In general, AB and CF reflectances will be referred to separately, but sometimes collectively as the PATMOS observations. The PATMOS grid-cell observations are collocated with AERONET ground-truth sites and used to retrieve the surface BRDF as well as τ_P.

b. AERONET data

The AERONET provides the ground-truth validation for this research. AERONET is a federation of sun–sky radiometers independently owned, but whose data are
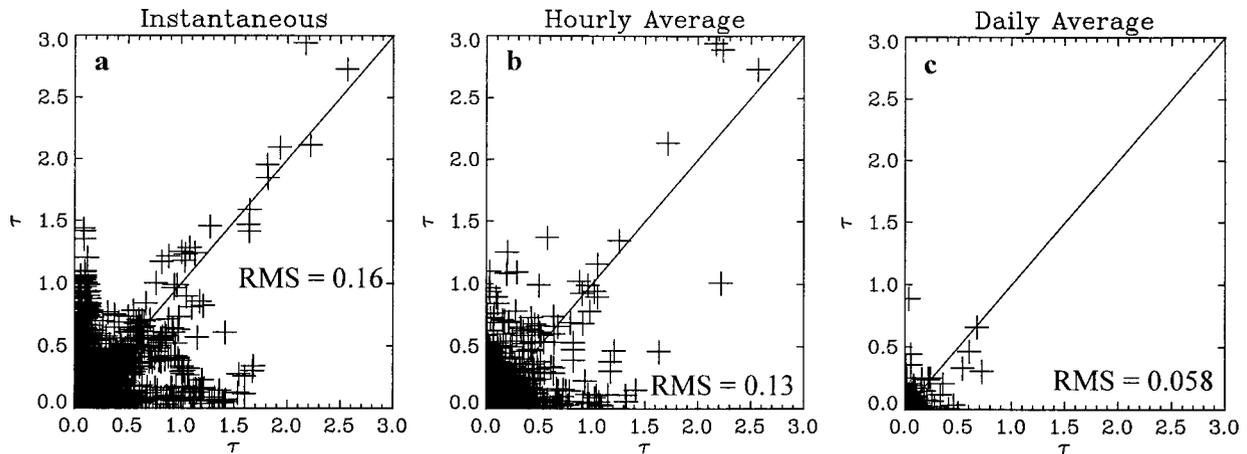
FIG. 2. Comparison of aerosol optical depths τ between AERONET sites in the same PATMOS grid cell demonstrating subgrid cell τ variability for (a) instantaneous observations, (b) hourly averages, and (c) daily averages. The solid line in each plot is the one-to-one correspondence line.

centrally archived. AERONET aerosol optical depths τ_A come from those sites where the data have been quality-controlled, cloud-cleared, and postcalibrated (i.e., level-2 data). They are estimated to have an accuracy of ±0.02 (Holben et al. 1998). The wavelengths λ observed by AERONET include 0.34, 0.38, 0.44, 0.50, 0.67, 0.87, and 1.02 μm. For this study, the aerosol optical depth (AOD) observations at these wavelengths are interpolated with a second-order polynomial fit in $\ln\lambda$ to $\lambda = 0.63$ μm, the effective central wavelength of AVHRR channel 1 and of the PATMOS retrievals.

For this study, PATMOS data from 1993 through 1999 are used, which matches the period of available observations from AERONET. Since the retrieval algorithm is developed for land areas, the nearest PATMOS grid cell with 100% land is selected for each AERONET site. AERONET sites not within 200 km of the center of a land-filled cell (e.g., islands) are excluded from this study.

Subgrid cell variability in τ_A

Since AERONET is compared with PATMOS retrievals, a potential source for uncertainty lies in the different spatial scales of each measurement due to aerosol spatial inhomogeneities. The magnitude of this uncertainty can be estimated by comparing AERONET observations that are located within the same PATMOS grid cells. Nine grid cells encompass more than one AERONET site. AERONET observations from sites within the same grid cell are intracompared in Fig. 2 for three different sampling times. Differences in the observations represent the subgrid-cell variability in τ_A, resulting from aerosol transport and local sources. The instantaneous observations show little correlation ($r = 0.51$), and temporal averaging (which decreases differences resulting from transport) offers marginal improvement ($r = 0.61$ and 0.56 for hourly and daily averaging, respectively). Also, the instanta-

neous, hourly-average and daily-average comparisons have rms differences between τ_A within a grid cell of 0.16, 0.13, and 0.058, respectively. The change in rms is largely due to the decrease in the range of τ at longer temporal averaging. However, as the comparisons show larger differences for shorter times, suggesting that subgrid-scale differences are being reduced by horizontal transport processes, some time averaging is employed when comparing τ_P with τ_A.

Based on this analysis, comparisons are made between nearly instantaneous PATMOS-retrieved τ_P and hourly-averaged AERONET observations centered on the PATMOS time τ_A. The hourly averaging reduces some of the spatial variation in τ within a grid cell while maintaining close correspondence in time with the AVHRR overpass. From these comparisons, one could expect the rms difference between τ_P and τ_A ($\Delta\tau$) to be no lower than 0.13. Conservatively, a value of 0.27 (twice this variability) is used as a reference point to assess PATMOS retrieval quality at each AERONET site. This value provides a context for the retrieval error assessment: τ_P retrievals whose random error (relative to τ_A) exceeds 0.27 (i.e., standard error of regression greater than 0.27) are considered affected by factors other than horizontal inhomogeneities in the aerosol (e.g., surface albedo variations).

c. Land cover classification

A land cover classification is used to assign retrieval accuracy to different land classes and to project PATMOS retrieval performance at AERONET sites to regions of matching surface type. DeFries and Townshend (1994) determined land cover classes by classifying temporal trends of NDVI in the AVHRR Pathfinder-Land dataset, which has a 1° latitude × longitude spatial resolution, closely matching PATMOS. Their 12 land classes are listed in Table 1 and shown in Fig. 3 (henceforth, DT

TABLE 1. NDVI-derived land cover classification from DeFries and Townshend (1994).

Land cover index	Classification
0	Water
1	Broadleaf evergreen forest
2	Coniferous evergreen forest and woodland
3	High-latitude deciduous forest and woodland
4	Tundra
5	Mixed coniferous forest and woodland
6	Wooded grassland
7	Grassland
8	Bare ground
9	Shrubs and bare ground
10	Cultivated crops
11	Broadleaf deciduous forest and woodland

land cover). The 83 AERONET sites used in the following comparisons are shown in Fig. 3 as crosses.

3. Aerosol retrieval from PATMOS data

The retrieval of aerosol information from the PATMOS data over land requires the simulation of numerous atmospheric and surface interactions. This section describes how the surface and atmosphere are numerically modeled and the process of retrieving the AOD.

a. Models

The Discrete Ordinate Radiative Transfer (DISORT) model (Stamnes et al. 1988) is used to simulate the interaction of solar radiation with the surface and atmosphere. Version 2 of DISORT was recently released and is used here for its ability to incorporate a surface BRDF.

Privette et al. (1997) found that the Rahman et al. (1993) BRDF model was most accurate for estimating spectral albedo and nadir reflectances for a variety of surfaces so it has been adopted. The Rahman BRDF model describes surface reflectance ρ_s at a given view zenith and azimuth angle (θ, ϕ) with solar illumination zenith and azimuth angles (θ_o, ϕ_o) via

$$\rho_s(\theta, \theta_o, \phi - \phi_o)$$

$$= \rho \, \frac{\cos^{k-1}\theta \, \cos^{k-1}\theta_o}{(\cos\theta + \cos\theta_o)^{1-k}}$$

$$\times \frac{1 - \Theta^2}{[1 + \Theta^2 - 2\Theta\cos(\pi - g)]^{3/2}} \left(1 + \frac{1 - \rho}{1 + G} \right), \quad (1)$$

where

$$G = [\tan^2\theta + \tan^2\theta_o - 2 \tan\theta \tan\theta_o \cos(\phi - \phi_o)]^{1/2}$$

$$g = \cos^{-1}[\cos\theta \cos\theta_o + \sin\theta \sin\theta_o \cos(\phi - \phi_o)],$$

and ρ, k, and Θ are the model parameters. Figure 4 shows how variations in the parameters affect the overall surface BRDF for savannah, which has $\rho = 0.019$, $k = 0.868$, and $\Theta = -0.241$ (Rahman et al. 1993). When viewing in the same direction as the illumination (i.e., when $\theta = \theta_o$ and $\phi - \phi_o = 0°$), the sharp increase in reflectance is known as the hot-spot effect and results from a minimum in the extent of shadows at this geometry.

Generally, the ρ parameter is a measure of the overall magnitude of reflectance (Fig. 4a). The k parameter defines the anisotropy; that is, it changes the relationship between the reflectance at the horizon and at the hot
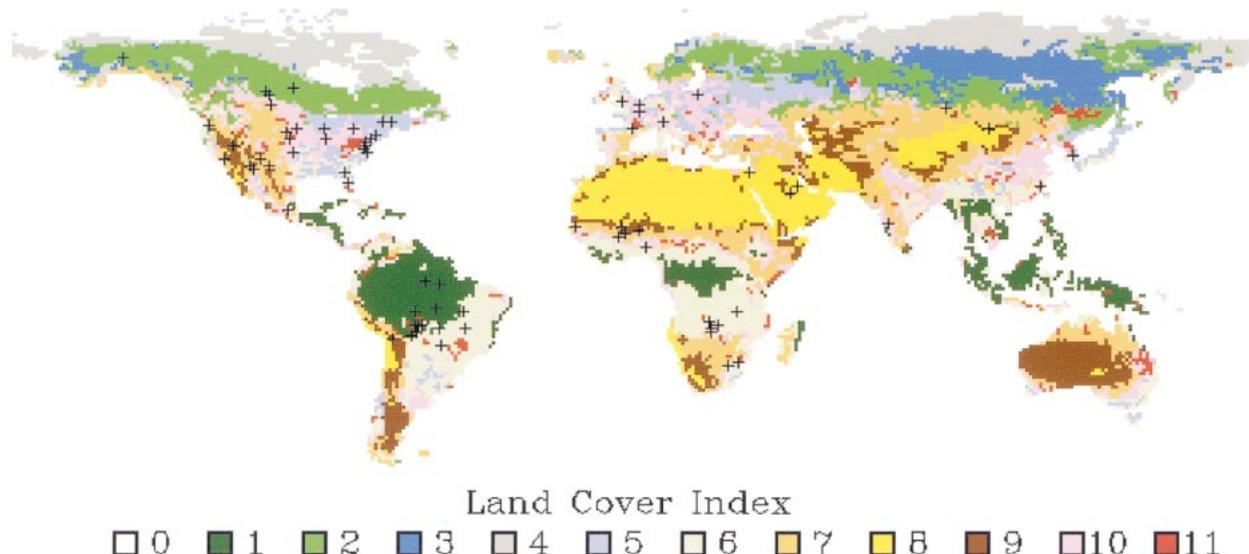

FIG. 3. DeFries and Townshend (1994) land cover index (see list in Table 1). Black crosses represent the AERONET sites used for retrieval validation.
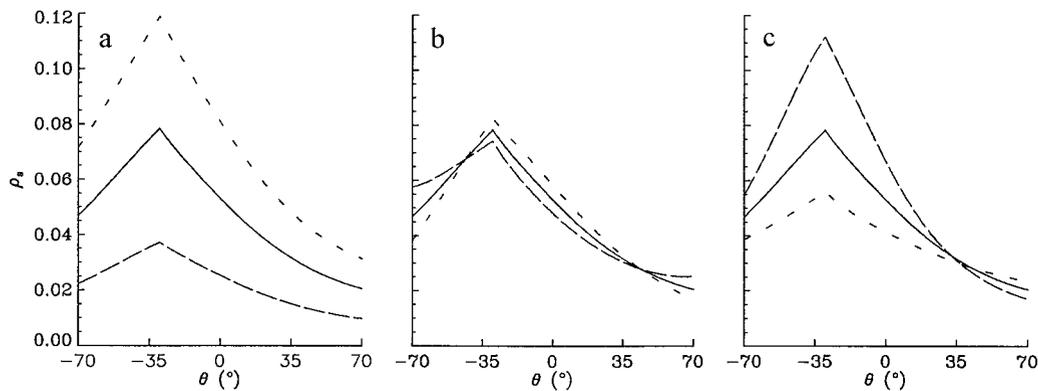
FIG. 4. The effect of varying BRDF parameters on the surface reflectance as a function of θ in the principal plane (where $\phi - \phi_o = 0°$ for $\theta < 0°$, backscattering) with sun at $\theta_o = 30°$. The solid line in all plots represents $\rho = 0.019$, $k = 0.868$, and $\Theta = -0.241$. Variations on these parameters are (a) $\rho = 0.009$ (short dash) and 0.029 (long dash), (b) $k = 0.968$ (short dash) and 0.768 (long dash), and (c) $\Theta = -0.441$ (short dash) and -0.041 (long dash).

spot (Fig. 4b). The Θ parameter (the Henyey–Greenstein function, which simulates multiple scattering in the canopy), affects the magnitude of the hot-spot effect, such that as Θ decreases, the reflectance in the hot-spot region increases (Fig. 4c). The ranges of k and Θ are [0, 1] and [−1, 1] respectively, while ρ is limited such that the hemispheric albedo of ρ_S is in the range [0, 1].

The aerosol retrieval method is being designed as a global algorithm to work for all PATMOS grid cells over land. In its initial form, the aerosol is simulated using a global aerosol model; that is, no spatial or temporal variations in the aerosol optical properties are included. Thus, comparisons of the retrievals with ground measurements are expected to show regional biases, which may be decreased by making regionally specific adjustments to this aerosol model. This is planned for subsequent versions. Currently, the aerosol is assumed to have a multimodal lognormal distribution of spherical particles based on the continental model described by Kaufman et al. (1997) and defined in Table 2. The complex refractive index used in the Mie scattering calculations is 1.4–0.005i, yielding a single-scatter albedo ω_o of 0.96. The remaining atmospheric properties are modeled using the tropical atmosphere (McClatchey et al. 1972).

An LUT is calculated using DISORT, which provides TOA reflectances calculated at numerous geometries for varying BRDF parameters and τ values. Ranges of angles and parameters used in the LUT are provided in

Table 3. Model reflectances at other values of parameters are estimated from interpolation in these LUTs.

b. Method

Because PATMOS cloud-free reflectances of land are primarily affected by the surface, the surface BRDF retrieval is at the heart of the aerosol algorithm. The surface BRDF retrieval is performed using a time series of PATMOS observations, called the composite time period (CTP). During the CTP, the TOA reflectances are sampled with respect to the dominant variable, view zenith angle θ. It is assumed by doing so, the aerosol contribution can be minimized by selecting the darkest observations at each θ. The darkest observations are then used with the LUT described above to select an optimum set of surface BRDF model parameters. Aerosol optical depth is then retrieved by matching each PATMOS observation with the theoretical TOA reflectance at that geometry using the retrieved surface BRDF parameters for that grid cell and CTP.

1) COMPOSITE TIME PERIOD DETERMINATION

The goal of the composite approach is to determine the surface BRDF parameters by viewing a location over

TABLE 2. List of the multimodal lognormal distribution parameters of the continental aerosol model (after Kaufman et al. 1997): mode radius, mode width, and number fraction f of the mode.

Mode	Radius (μm)	Width	f
1	0.005	2.97	0.35
2	0.500	2.97	0.00001
3	0.012	2.00	0.65

TABLE 3. List of parameters with their range and discrete steps (Δ) in the LUT.

Parameter	Min	Max	Δ	No.
θ_o	10°	70°	5°	13
θ	0°	70°	5°	15
$\phi - \phi_o$	0°	180°	10°	19
ρ	0.005	0.15	0.005	30
k	0.0	1.0	0.1	11
Θ	−.95	.95	0.2	10
τ	0.01	2.56	Variable*	9

* The τ values increase geometrically: 0.01, 0.02, 0.04, 0.08, 0.16, 0.32, 0.64, 1.28, and 2.56.

a long enough time that cloud-free reflectances minimally affected by aerosols can be collected over many viewing zenith angles. However, the time period must be short enough such that the surface properties do not significantly change. The AVHRR observes a location from eight distinct viewing geometries in an 8-day repeat cycle, so several cycles need to be collected to increase the chance for minimal aerosol conditions to be present. The CTP is determined by grouping these repeat cycles and counting the number of cloud-free observations in each of the eight observation angle bins (with width $\Delta \theta \sim 15°$). The CTP is defined as the shortest length of time (not to exceed 48 days) that provides at least three CF observations in half of the view angle bins. This "repeat cycle" (RC) method is similar to that used by O'Brien et al. (1998) in retrieving surface BRDF parameters at semiarid sites in Australia.

To increase the number of observations in an observation angle bin, a secondary CTP calculation is performed where monthly composites are used to retrieve surface parameters. In recent retrievals of surface albedo from AVHRR (e.g., Csiszar and Gutman 1999), numerous years have been composited together to estimate monthly mean albedo. This second "fixed monthly" (FM) method uses daily cloud-free reflectances from the same month of the year, for the period 1993–99, as a CTP. This increases the number of observations in a CTP into the hundreds. As a result, it may likely provide a more accurate BRDF retrieval than the RC–CTP because of the larger number of observations in each viewing bin at different solar zenith and relative azimuth angles. However, it is more susceptible to errors caused by residual long-term calibration drift and interannual changes in the surface reflectance.

2) SURFACE BRDF RETRIEVAL

For each CTP, the model-generated LUT is interpolated to the specific geometry of each observation using an aerosol optical depth τ_b which represents the background aerosol still present on the "cleanest" days (assumed to be $\tau_b = 0.05$). For each observation geometry (θ, θ_o, ϕ), the modified LUT has 3300 possible TOA reflectances, one for each combination of the three BRDF model parameters ρ, k, and Θ. The BRDF parameters are retrieved for the CTP by selecting the parameter set yielding the minimum cost function, C_j:

$$ C_j = \frac{\sum_i \left[\frac{(R_{\text{sat},i} - R_{\text{LUT},i,j})}{\sigma_{R,i}} w_i \right]^2 + P_{i,j}}{\sum_i w_i}, \quad (2) $$

where j represents one of the 3300 BRDF combinations; i is an individual observation (i.e., day) in the CTP; $R_{\text{sat},i}$ is the PATMOS observed reflectance on day i; $R_{\text{LUT},i,j}$ is the LUT reflectance for BRDF combination j interpolated to the geometry on day i; $\sigma_{R,i}$ is the standard de-
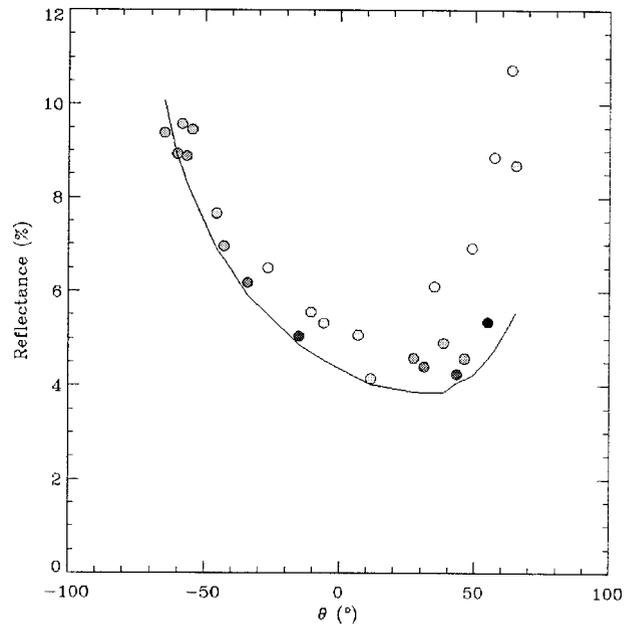

FIG. 5. PATMOS AB reflectances vs θ during an RC–CTP at Alta Floresta, with TOA reflectance from the BRDF parameter set with the minimum C_j shown by the line. The shading of the circles is proportional to w_i [used in Eq. (2)].

viation of the pixel reflectance observations in the grid cell on day i; w_i is the weight assigned to the $R_{\text{sat},i}$; and $P_{i,j}$ is a penalty function defined as

$$ P_{i,j} = \begin{cases} 10 & R_{\text{sat},i} < R_{\text{LUT},i,j} \\ 0 & R_{\text{sat},i} > R_{\text{LUT},i,j}. \end{cases} \quad (3) $$

This cost function differs from other retrieval cost functions by the inclusion of w_i and $P_{i,j}$. The weight is computed using the range of reflectances in each angular bin such that larger weight is assigned to observations at the lower end of the range. This has the effect of selecting the BRDF parameters that match the darker observations in each angular bin. Since minimal τ_b is assumed, few cloud-free observations should have lower reflectances than those simulated. Therefore, a penalty function is included to rule out (ρ, k, Θ) combinations that closely match, but are brighter than the observations. The penalty is only applied when a BRDF combination satisfies this condition on more than one day, so the method allows for one observation to be darker than the LUT. The surface BRDF parameter set yielding the minimum C_j is the retrieved set used for that CTP. An example of the BRDF parameter retrieval is shown in Fig. 5. The AB reflectances (circles) show R_{sat} increasing toward the hot spot and becoming more variable at $\theta > 30°$. The shading of the circles is proportional to w_i such that darker circles have larger weights. The TOA reflectances associated with the parameter set with the minimum C_j ($\rho = 0.01$, $k = 0.4$, and $\Theta = -0.3$) follows the lower R_{sat} values extremely well.
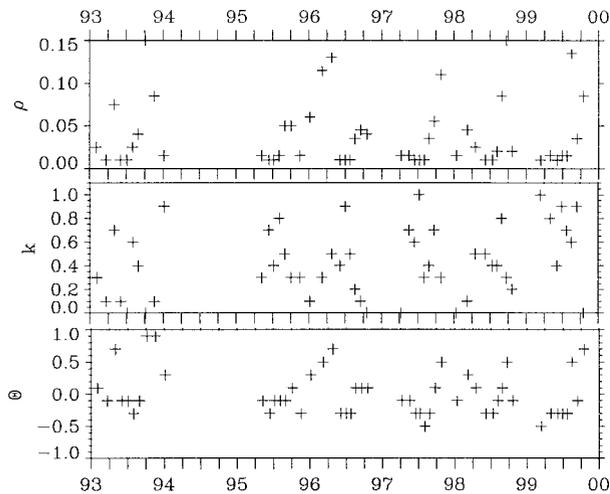
FIG. 6. Time series of retrieved BRDF parameters at Alta Floresta for each RC–CTP from 1993 through 1999 for AB reflectances.

FIG. 7. BRDF parameters retrieved using the FM–CTP method at Alta Floresta for AB reflectances.

A time series of the retrieved BRDF parameters using the repeat cycle CTP is shown in Fig. 6 for Alta Floresta (located in South America) from 1993–99. While this site is located in a broadleaf evergreen forest (i.e., rain forest) and the reflectance, as such, can be characterized as relatively constant over the year (Gutman 1999; DeFries and Townshend 1994), ρ shows significant variability, ranging from 0.01 to 0.14. The AERONET aerosol optical depths at some sites near the biomass burning rarely fall below 0.5 during the burning season (July–September). Thus, these persistently elevated τ values are likely causing the surface BRDF retrieval to overestimate ρ. The ρ retrieved using the FM–CTP method (Fig. 7) shows much less variation, having a maximum of only 0.05 in October, possibly due to surface changes during this dry season or residual persistent smoke.

3) AEROSOL OPTICAL DEPTH RETRIEVAL

Variation between R_{sat} and R_{LUT} (i.e., between the circles and the solid line in Fig. 5) is assumed to be the aerosol signal. Aerosol optical depth τ_P for each day's grid-cell mean reflectance is retrieved by interpolating in the set of precomputed LUTs (cf. Table 3) such that $R_{sat} = R_{LUT}$. The retrieved optical depths τ_P are reported using a subscript identifying the BRDF retrieval method (RC or FM) and the PATMOS reflectances (CF or AB) described above.

c. Summary of assumptions in the retrieval method

As in most satellite retrievals, the estimation of aerosol optical depth from PATMOS data is an underdetermined system that requires assumptions on the properties of the aerosols, surface, and observations. The following is a list of assumptions made with the present algorithm.
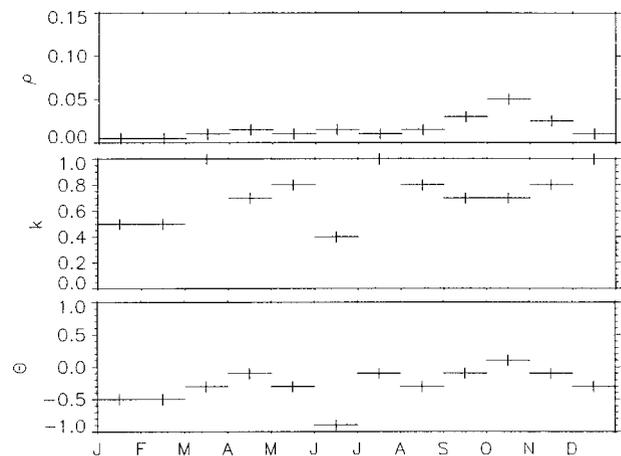
- The size distribution and chemical composition (i.e., the index of refraction) are assumed to be modeled by the information provided in Table 2; variations from this will likely cause biases at different sites depending on the average properties of the aerosol in that region.
- The shape of the aerosol is assumed spherical and the vertical distribution is assumed to be at a maximum in the lowest 3 km of the atmosphere, with much less in the free troposphere and stratosphere. These assumptions are invalid where contribution from dust is a large portion of the optical depth or significant transport occurs through lofting of the aerosol layer. The assumed vertical distribution will cause little error except in the cases of large absorption.
- It is assumed that the surface can be modeled by a Rahman BRDF.
- The surface properties within the grid cell are assumed constant during the CTP. In a case where the surface changes significantly—which is quite possible with the FM method—the results would likely show large biases.
- The surface of the grid cell is assumed to have sufficient homogeneity that observations from different days have limited variation in surface properties. This arises from the nature of the grid-cell averaging; clouds in the grid cell will obscure different parts of the grid cell on different days. This could cause large variations in the actual surface that is observed. In cases where the surface is vastly heterogeneous, the retrieval method will produce large positive bias and enhanced noise.
- It is assumed that aerosols increase the PATMOS-observed reflectances. Instances where this is invalid will show large positive bias and possible anticorrelation between τ_P and τ_A, which is more likely in regions of bright surfaces or absorbing aerosols.
- It is assumed that the PATMOS reflectances have neg-

ligible residual calibration drift after vicarious cali-
bration corrections are made. If this is wrong, it will
likely cause bias, especially in retrievals using the FM
method, which uses observations from 7 yr of data.

- The CLAVR cloud screening algorithm sufficiently
  removes all clouds. No cloud mask is perfect; how-
  ever, the CLAVR algorithm works extremely well dur-
  ing the daytime. Any residual cloud effects will cause
  large positive errors and are more likely to occur in
  the CF reflectances due to the selection of the darker
  observations for the AB pixels.
- The grid cell must be sufficiently sampled in time to
  yield observations with little aerosol present. Increas-
  ing the number of observations will increase the like-
  lihood of observing the background aerosol, but this
  increases the chance that the surface is changing. If
  τ_b is too low, the cloud-free reflectances will yield a
  ρ that is too high and possibly change the k and Θ
  parameters as well. In comparisons to ground truth,
  it would increase the occurrence of negative errors
  (i.e., where $\tau_P \sim 0$ and $\tau_A > 0$).
- The gaseous absorption variations are assumed neg-
  ligible. For AVHRR channel 1 (0.63 μm), ozone ab-
  sorption is small, so daily variations in ozone will
  only slightly affect the comparisons.

Next, four retrieval methods are discussed which de-
rive from two CTP methods (FM and RC) and the two
cloud-free PATMOS reflectances (CF and AB). Retriev-
al methods are validated with AERONET to determine
which is most accurate.

4. Results

BRDF parameters and daily optical depths τ_P for var-
ious composite time periods are retrieved from PAT-
MOS observations between 1993 and 1999 at more than
80 AERONET sites. On days with at least one AERO-
NET observation within a half-hour of the satellite over-
pass, τ_A is compared to τ_P, which results in more than
5000 match-ups globally (for grid cells with more than
one AERONET site, the τ_A from each site is indepen-
dently compared to τ_P). Discussion of results is limited
to one case study and a global analysis for all sites using
regression statistics. First, however, the results of the
BRDF retrieval are discussed.

a. Surface BRDF retrieval

The retrieval of accurate surface BRDF parameters
is required for the retrieved τ to be accurate. However,
as no ground truth exists for BRDFs at the scale of
PATMOS grid cells, its validation is limited to consis-
tency checks of the retrieved parameters. The average
BRDF parameters for each site using the AB–FM meth-
od are plotted as a function of land-cover type in Fig.
8 (see the plus sign in Fig. 3 for location). In general,
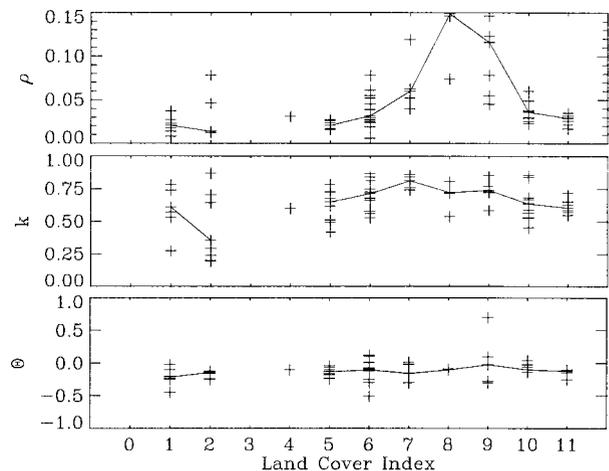the parameters are within the LUT ranges, that is, not

FIG. 8. Average retrieved surface BRDF parameters from the AB–
FM method grouped by DT land cover index for all comparison
AERONET sites. The medians for each index are connected by a
line.

grouped at one boundary, which suggests no significant
biases in the retrieval algorithm. The exception is ρ; for
most bare ground sites (DT index = 8), it is near 0.15
(the upper limit of the LUT), which suggests that ρ may
actually be higher in these areas. The values of k and
Θ are similar to those reported by Rahman et al. (1993;
k is generally greater than 0.5 and Θ ranges from -0.4
to about 0.2), where the BRDF model is fit to reflectance
observations from numerous surface types. The ρ pa-
rameter shows the largest variation with land cover;
darker sites are located in forested areas and brighter
sites in less vegetated areas (cf. Table 1). Further ver-
ification of the BRDF parameters is outside the scope
of this article. The remaining validation is dedicated to
the retrieval of aerosol optical depth.

b. Aerosol optical depth retrieval

The success of the retrieval method can best be mea-
sured by the amount of scatter between τ_P and τ_A. Bi-
ases—either a linear regression offset (b) other than zero
or a slope (m) other than one—can possibly be corrected
by changing the aerosol optical properties, BRDF model
parameters, instrument calibration or the retrieval meth-
od itself. However, noise—represented by a low cor-
relation coefficient r or a large standard error of re-
gression ε—represents a fundamental weakness of the
retrieval concept, that is, a physical limitation such as
high surface reflectance. The initial objective of this
validation is to determine where (and for which land
surface types) significant noise will render aerosols un-
detectable from single-channel reflectance measure-
ments of AVHRR.

1) CASE STUDY—ALTA FLORESTA, BRAZIL

Alta Floresta is located in a region of rain forest
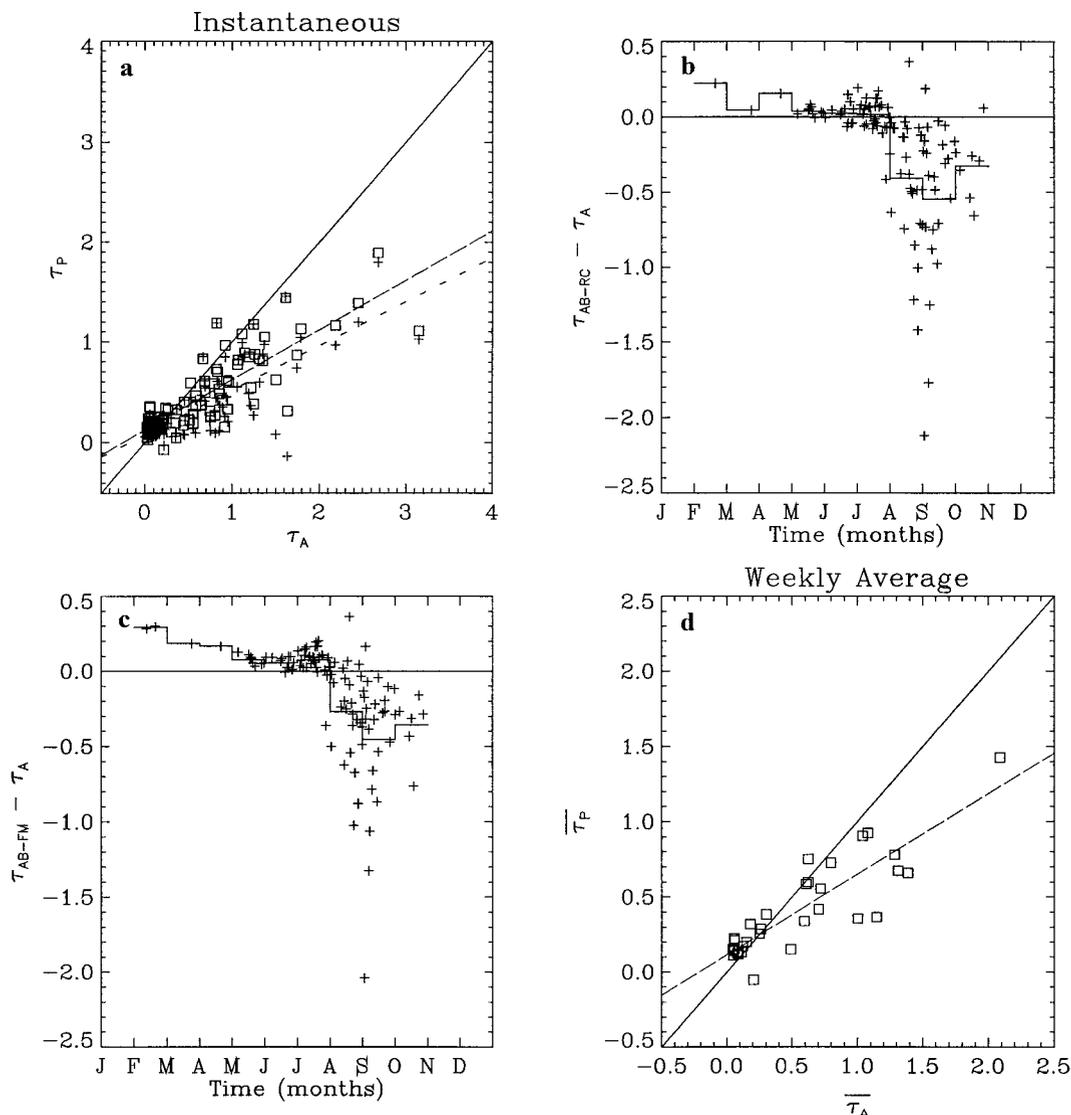(broadleaf evergreen forest land cover) in western Bra-

FIG. 9. (a) Validation of two retrievals with AERONET data at Alta Floresta: crosses represent τ_{AB-RC} and squares τ_{AB-FM}. The solid line is the 1:1 correspondence line and the long and short-dashed lines are the linear regressions for τ_{AB-FM} and τ_{AB-RC}, respectively. (b) Retrieval error ($\tau_{AB-RC} - \tau_A$) vs time of year (with monthly median connected by line). (c) Retrieval error ($\tau_{AB-FM} - \tau_A$) vs time of year (with monthly median connected by line). (d) Weekly average of τ_{AB-FM} vs τ_A where dashed line is the linear regression and solid line is 1:1 correspondence.

zil. Local aerosols are dominated by biomass burning that occurs between late July and September of each year (Prins et al. 1998). The comparisons of τ_{AB-RC} and τ_{AB-FM} retrievals with τ_A are shown in Fig. 9a. The corresponding linear regression statistics for all four retrieval methods are provided in Table 4. The correlation is larger and ε is smaller for the FM–CTP method, independent of which PATMOS reflectance is used. Thus, it is concluded from this initial retrieval attempt that the FM retrieval at Alta Floresta shows the strongest sensitivity to aerosol signal. The biases relative to AERONET (slope less than one and intercept greater than zero) can possibly be removed by adjusting the retrieval mod-

el parameters, but this will be the subject of another paper.

The retrieval errors show significant temporal trends at this location. The τ_{AB-RC} retrieval error (i.e., $\tau_{AB-RC} - \tau_A$) is plotted versus day-of-year (independent of year, 1993–99) in Fig. 9b (and for τ_{AB-FM} in Fig. 9c). The retrieval errors exhibit large negative biases during the biomass burning season of July through September. This may be partly due to insufficient absorption in the aerosol model or because the aerosol smoke plume has a much larger and interannually persistent background optical depth than that assumed in the BRDF retrieval (τ_b, described above). This causes the aerosol signal to be

TABLE 4. Statistics for the validation at Alta Floresta for each retrieval method: linear regression correlation *r*, slope *m*, intercept *b*, and standard error of estimate ε.

	RC		FM		Weekly average FM
	CF	AB	CF	AB	AB
r	0.72	0.73	0.87	0.86	0.87
m	0.39	0.40	0.55	0.50	0.54
b	0.10	0.06	0.16	0.13	0.11
ε	0.23	0.23	0.19	0.18	0.16

included in the surface BRDF retrieval and thereby underestimates τ even with the FM method. The $\tau_{\text{AB–FM}}$ errors (Fig. 9c) show slightly less negative bias during the burning season, but significantly larger positive biases in other months (e.g., March–May). Thus while $\tau_{\text{AB–FM}}$ correlates better with AERONET, it seems to have greater seasonal biases. Attempts are under way to reduce these biases by using regionally specific information about the aerosol from global climatologies.

Finally, weekly averaging is performed to see what impact it has, since climatologies often are comprised of time-averaged data to reduce random variations. The weekly averaged AB–FM retrieval is compared to the weekly averaged AERONET τ_A (Fig. 9d); linear regression statistics are provided in Table 4. The results show a slight decrease in noise and little change in slope or intercept for Alta Floresta. Overall, weekly averaging does increase the correlation with τ_A at 70% of the sites analyzed.
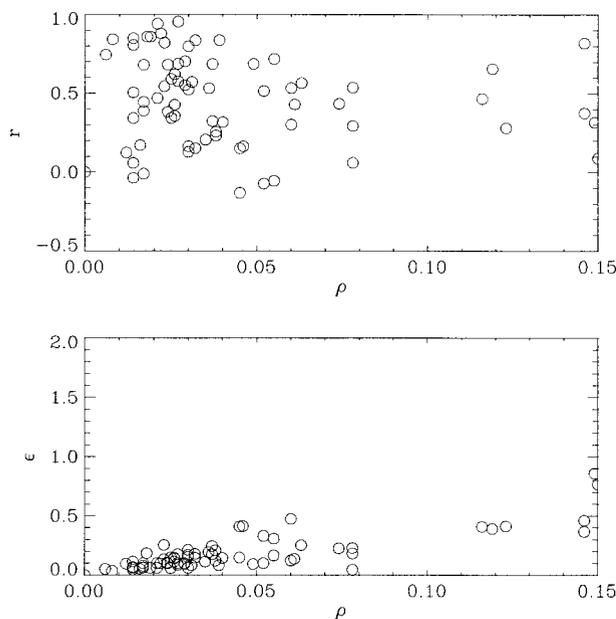

FIG. 10. Retrieval *r* and ε vs average retrieved ρ at each AERONET site for $\tau_{\text{AB–FM}}$.

TABLE 5. Median *r* grouped by land cover type for the two retrieval runs (RC and FM) and both PATMOS reflectances (CF and AB) along with the number of AERONET sites *N* in each land cover type. No AERONET sites were located in land cover types 3 or 4 so they are not included in further analysis.

		Model run			
		RC		FM	
		PATMOS reflectance from			
Index	*N*	CF	AB	CF	AB
1	9	0.69	0.79	0.75	0.84
2	9	0.26	0.25	0.22	0.34
5	10	0.41	0.51	0.58	0.47
6	17	0.45	0.59	0.54	0.69
7	7	0.45	0.23	0.56	0.32
8	4	0.22	0.27	0.37	0.38
9	7	0.06	0.13	0.15	0.47
10	12	0.38	0.47	0.49	0.52
11	8	0.43	0.42	0.40	0.43

2) GLOBAL ANALYSIS

The method with the greatest ability to retrieve aerosol optical depth from PATMOS reflectances is being identified with the largest *r* and smallest ε values from the statistical comparison between the AERONET- and PATMOS-retrieved τ. Overall, this ability is generally better over darker surfaces as shown in Fig. 10. Although *r* seems relatively independent of ρ (Fig. 10a), ε is significantly less when $\rho < 0.04$. This decrease in error over darker surfaces is related to the land cover type within the PATMOS grid cell.

The median correlation coefficients between τ_P and τ_A from all AERONET sites and for the four BRDF retrieval algorithms, grouped by land cover type, are provided in Table 5. The results are similar to those at Alta Floresta, that is, larger correlations for AB–FM retrievals. The largest median correlation occurs for the AB–FM retrieval in six of the nine surface types. The median ε for each retrieval and each land cover type is provided in Table 6 (similar to Table 5). Lowest noise

TABLE 6. Median ε grouped by land cover type for the two retrieval runs (RC and FM) and both PATMOS reflectances (CF and AB) along with the number of AERONET sites *N* for each land cover type.

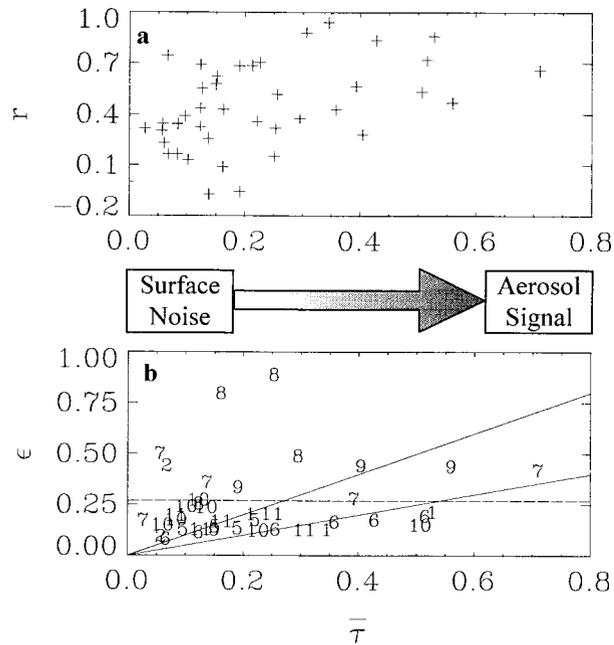|		Model run			
		RC		FM	
		PATMOS reflectance from			
Index	*N*	CF	AB	CF	AB
1	9	0.17	0.12	0.17	0.18
2	9	0.09	0.06	0.07	0.07
5	10	0.12	0.09	0.12	0.10
6	17	0.14	0.08	0.11	0.10
7	7	0.24	0.35	0.25	0.33
8	4	1.18	1.05	0.90	0.77
9	7	0.44	0.54	0.38	0.41
10	12	0.17	0.14	0.18	0.15
11	8	0.14	0.10	0.15	0.11

Fig. 11. (a) Correlation coefficient and (b) standard estimate of error ε for each AERONET site validation using τ_{AB-FM}. The dashed line represents the $\varepsilon = 0.27$ value. The solid lines delineate regions of 50% and 100% error ($\varepsilon/\bar{\tau} \times 100$) and the numbers represent the DT land cover class.

estimates occur with the AB–RC retrieval. However, the range of noise between different retrieval methods is small, with that of the AB–FM retrieval generally within ± 0.05 of the minimum noise for each land cover type.

The noise levels also vary between land classes. For example, the coniferous evergreen forest and woodland (DT index = 2) shows generally low correlations ($r < 0.42$) yet with low noise ($\varepsilon < 0.09$). This effect can also be seen in Fig. 11, where r and ε for each AERO-NET site are plotted versus the average τ_A ($\bar{\tau}$) at that site. The correlation coefficient increases with $\bar{\tau}$; how-ever, ε shows little dependence on $\bar{\tau}$. Therefore, retriev-als may be valid for certain sites where ε is small, in spite of a low r, because the correlation is more de-pendent on the range of τ_A.

Results in Fig. 11 also demonstrate the transition of comparisons dominated by surface noise ($\tau < 0.2$) to those dominated by aerosol signal ($\tau > 0.4$). Retrievals relative to τ show errors greater than 100% at $\tau < 0.3$ and more retrievals with errors less than 50% as τ in-creases past 0.4. Also, it is clear that the largest errors are associated with desert (i.e., bare ground: DT = 8) sites. Generally, DT = 7, 8, and 9 have errors in excess of 0.27 and therefore are likely to have significant sur-face reflectance spatial inhomogeneities.

The median ε for the AB–FM retrieval (cf. Table 6) has been used to map the global potential for the τ retrieval over all land surface types in Fig. 12, where τ retrievals have larger potential for land cover types with smaller ε values. The portion of land with $\varepsilon < 0.27$ (i.e., less potential of surface reflectance inhomogene-ities impacting a retrieval) is 78%.

However, this may be a conservative estimate of the global potential for aerosol retrieval over land. The sur-face BRDF is generally brighter for $\theta < 0°$, that is, viewing the hot-spot side (cf. Fig. 4), which causes a
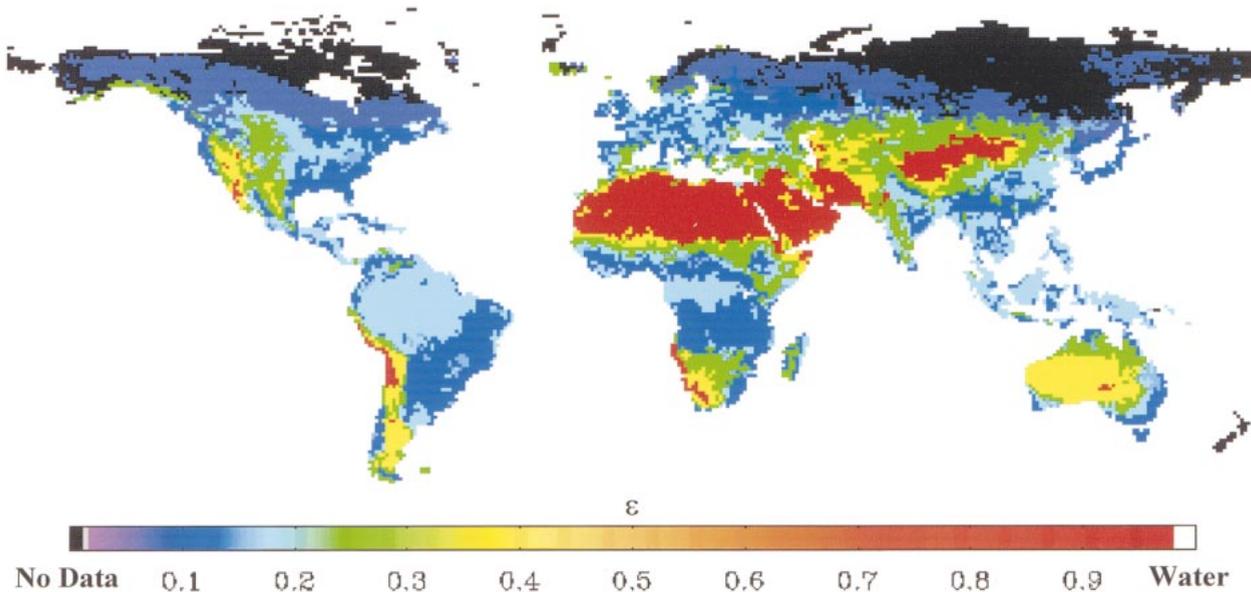

Fig. 12. Global potential for the retrieval of aerosols over land from PATMOS data based on an extrapolation of the median ε of each land type from Table 6 to a map of land cover type (Fig. 3) where black represents surface types where no validation sites were available. Retrieval potential is inversely proportional to ε; $\varepsilon = 0.27$ is a threshold above which subgrid-scale variations in surface reflectance can adversely affect the aerosol retrieval (i.e., low potential).
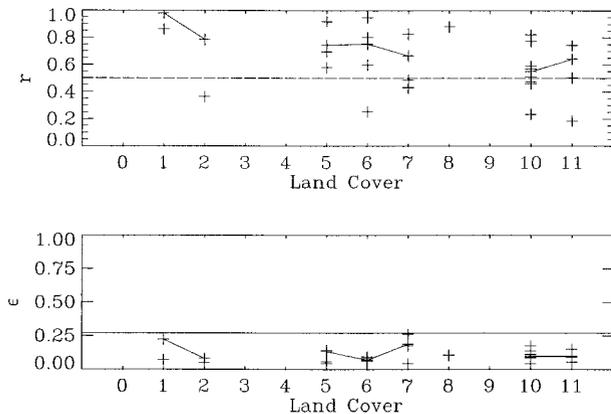
FIG. 13. Retrieval validation (r and ε) at AERONET sites grouped by land cover using a subset of the AB–FM retrievals having observations with $\theta > 0°$, NCF > 400, and $\rho < 0.10$.

decreased sensitivity to changes in τ in the PATMOS observations. Also, the number of cloud-free pixels in the PATMOS grid cell range from 100 to 1000. By limiting comparisons to those grid cells where a large portion of the grid cell is cloud-free, the observed mean reflectance is more likely to be consistent with τ_A. The results, r and ε, grouped by land cover type are presented in Fig. 13 where comparisons include only those observation that satisfy: $\theta > 0°$, number of CF pixels > 400 and $\rho < 0.10$. Significantly higher correlations and lower ε are found for most sites (cf. Tables 5, 6). Therefore, the estimated global potential for the retrieval (Fig. 12) can be enhanced by adding constraints to the method.

5. Conclusions

Aerosol optical depth was retrieved at more than 80 AERONET sites around the globe using PATMOS cloud-free and aerosol-burden reflectances from 1993 through 1999. The surface bidirectional reflectance distribution function was retrieved using a lookup table created using the DISORT radiative transfer model with an assumed background aerosol optical depth coupled with the Rahman BRDF model. Optical depths were then retrieved using the retrieved BRDF parameters and the PATMOS reflectances assuming a globally constant aerosol. Retrievals were made using the two clear-sky reflectances from the PATMOS data and two time compositing methods. The PATMOS and AERONET retrievals were statistically compared through regression analysis to estimate which method might perform better globally. Regression results are grouped by land cover type at the AERONET sites, which allowed a global extrapolation of the retrieval potential (considered to be inversely proportional to the standard error of regression).

The results of this research show that it may be possible to retrieve aerosol information over many land cover classes representing 78% of all land areas. The implications of this success are far reaching. The AVHRR PATMOS grid-cell-averaged data may be used to supply daily aerosol optical depths over most land areas from 1981 through the present. This has a significant impact on international efforts to produce a global aerosol climatology. Highest retrieval accuracy (high correlation and low noise) occurs in grid cells with dark uniform vegetation (e.g., heavily vegetated areas). Some retrieval success was also found over grasslands and deciduous forests. Conversely, little success was found in desert (i.e., bare ground) regions.

Retrieval accuracy will likely be improved by planned further research. The inclusion of regional characterization of aerosol optical properties in the LUT would likely remove systematic biases. Also, current calculations fix the Rayleigh scattering optical depth; this varies little with time but changes significantly with the altitude of a grid cell. The inclusion of information on the growth cycle of the vegetation (perhaps from analysis of channel-2 reflectance at 0.83 μm) could possibly avoid confusing persistent biomass burning with seasonal changes in the surface BRDF.

Overall, the primary retrieval strengths are as follows.

- It can be validated at AERONET sites and also against other estimates of aerosol burden (e.g., other solar radiation datasets, visibility observations).
- The long time record allows the determination of seasonal surface BRDF patterns.
- Retrieval correlation is highest over rain forests and evergreen land classes. The rain forests are best for validation because biomass burning provides a large and variable aerosol signal.
- There are observational criteria that can be used to decrease the uncertainty of the retrievals.
- Seventy-eight percent of land surfaces show a strong potential for detecting aerosol optical depth.

However, the retrieval algorithm has drawbacks as well.

- Desert areas and other bright surfaces result in retrievals that are poorly correlated with AERONET and have large standard errors of estimate.
- There is some success over grasslands and other land types, although the random error (roughly 0.2–0.3) is comparable to the size of the aerosol signal for most regions.
- Seasonal variations in biomass burning can be mistaken as seasonal changes in surface reflectance, which increases the noise and systematic error of the retrieval.

Nonetheless, these preliminary results show that an ability exists for deriving aerosol optical depth information from the PATMOS data over land. Results suggest the possibility of using this algorithm to detect aerosol events where the signal is large and widespread (enough to cover a 110×110 km^2 grid cell) particularly

over a dark background; aerosol sources that satisfy these conditions include biomass burning and industrial pollution.

REFERENCES

Csiszar, I., and G. Gutman, 1999: Mapping global land surface albedo from NOAA AVHRR. *J. Geophys. Res.,* **104** (D6), 6215–6228.

Deering, D. W., T. F. Eck, and B. Banerjee, 1999: Characterization of the reflectance anisotropy of three boreal forest canopies in spring–summer. *Remote Sens. Environ.,* **67,** 205–229.

DeFries, R. S., and J. R. G. Townshend, 1994: NDVI-derived land cover classification at a global scale. *Int. J. Remote Sens.,* **15,** 3567–3586.

Fraser, R. S., 1993: Optical thickness of atmospheric dust over Tadzhikistan. *Atmos. Environ.,* **27A,** 2533–2538.

——, and Y. J. Kaufman, 1985: The relative importance of aerosol scattering and absorption in remote sensing. *IEEE Trans. Geosci. Remote Sens.,* **23,** 625–633.

Gutman, G., 1999: On the use of long-term global data of land reflectance and vegetation indices derived from the advanced very high radiometer. *J. Geophys. Res.,* **104** (D6), 6241–6255.

Higurashi, A., T. Nakajima, B. N. Holben, A. Smirnov, R. Frouin, and B. Chatenet, 2000: A study of global aerosol optical climatology with two-channel AVHRR remote sensing. *J. Climate,* **13,** 2011–2027.

Hindman, E. E., P. A. Durkee, P. A. Sinclair, and T. H. Vonder Haar, 1984: Detection of marine aerosol in coastal zones using satellite imagery. *Int. J. Remote Sens.,* **5,** 577–586.

Holben, B. N., E. Vermote., Y. J. Kaufman., D. Tanré, and V. Kalb, 1992: Aerosol retrieval over land from AVHRR data—Application for atmospheric correction. *IEEE Trans. Geosci. Remote Sens.,* **30,** 212–222.

——, and Coauthors, 1998: AERONET—A federated instrument network and data archive for aerosol characterization. *Remote Sens. Environ.,* **66,** 1–16.

Husar, R. B., J. M. Prospero, and L. L. Stowe, 1997: Characterization of tropospheric aerosols over the oceans with the NOAA advanced very high-resolution radiometer optical thickness product. *J. Geophys. Res.,* **102,** 16 889–16 909.

Jacobowitz, H., 1999: AVHRR PATMOS datasets available online from NOAA. *Bull. Amer. Meteor. Soc.,* **80,** 967–968.

Justice, C. O., T. F. Eck, D. Tanré, and B. N. Holben, 1991: The effect of water vapour on the normalized difference vegetation index derived for the Sahelian region from NOAA AVHRR data. *Int. J. Remote Sens.,* **12,** 1165–1187.

Kaufman, Y. J., 1987: Satellite remote sensing of aerosol absorption. *J. Geophys. Res.,* **92,** 4307–4317.

——, and J. H. Joseph, 1982: Determination of surface albedos and aerosol extinction from characteristics from satellite imagery. *J. Geophys. Res.,* **87,** 1287–1299.

——, R. S. Fraser, and R. A. Ferrare, 1990: Satellite measurement of large-scale air pollution: Methods. *J. Geophys. Res.,* **95,** 9895–9909.

——, D. Tanré, L. A. Remer, E. F. Vermote, A. Chu, and B. N. Holben, 1997: Operational remote sensing of tropospheric aerosol over land from EOS moderate-resolution imaging spectro-radiometer. *J. Geophys. Res.,* **102,** 17 051–17 068.

Li, Z., J. Cihlar, X. Zheng, L. Moreau, and H. Ly, 1996: The bidirectional effects of AVHRR measurements over boreal regions. *IEEE Trans. Geosci. Remote Sens.,* **34,** 1308–1322.

McClatchey, R. A., R. W. Fenn, J. E. A. Selby, F. E. Volz, and J. S. Garing, 1972: Optical properties of the atmosphere. Air Force Cambridge Research Laboratory Res. Paper 354, 108 pp.

Mishchenko, M. I., I. V. Geogdzhayev, B. Cairns, W. B. Rossow, and A. A. Lacis, 1999: Aerosol retrievals over the ocean by use of channels 1 and 2 AVHRR data: Sensitivity analysis and preliminary results. *Appl. Opt.,* **38,** 7325–7341.

Mitchell, R. M., and D. M. O'Brien, 1993: Correction of AVHRR shortwave channels for the effects of atmospheric scattering and absorption. *Remote Sens. Environ.,* **46,** 129–145.

O'Brien, D. M., R. M. Mitchell, M. Edwards, and C. C. Elsum, 1998: Estimation of BRDF from AVHRR short-wave channels: Tests over semiarid Australian sites. *Remote Sens. Environ.,* **66,** 71–86.

Prins, E. M., J. M. Feltz, W. P. Menzel, and D. E. Ward, 1998: An overview of *GOES-8* diurnal fire and smoke results for SCAR-B and 1995 fire season in South America. *J. Geophys. Res.,* **103,** 31 821–31 835.

Privette, J. L., C. Fowler, G. A. Wick, D. Baldwin, and W. J. Emery, 1995: Effects of orbital drift on advanced very high-resolution radiometer products: Normalized difference vegetation index and sea surface temperature. *Remote Sens. Environ.,* **53,** 164–171.

——, T. F. Eck, and D. W. Deering, 1997: Estimating spectral albedo and nadir reflectance through inversion of simple BRDF models with AVHRR/MODIS-like data. *J. Geophys. Res.,* **102,** 29 529–29 542.

Rahman, H., and G. Dedieu, 1994: SMAC: A simplified method for the atmospheric correction of satellite measurements in the solar spectrum. *Int. J. Remote Sens.,* **15,** 123–143.

——, B. Pinty, and M. M. Verstraete, 1993: Coupled Surface–Atmosphere Reflectance Model 2. Semiempirical surface model usable with NOAA advanced very-high resolution radiometer data, *J. Geophys. Res.,* **98,** 20 791–20 801.

Rao, C. R. N., and J. Chen, 1995: Intersatellite calibration linkages for the visible and near-infrared channels of the advanced very high-resolution radiometer on the *NOAA-7, NOAA-9,* and *NOAA-11* spacecraft. *Int. J. Remote Sens.,* **16,** 1931–1942.

Schussel, G., R. E. Dickinson, J. L. Privette, W. J. Emery, and R. Kokaly, 1994: Modeling the bidirectional reflectance distribution function of mixed finite plant canopies. *J. Geophys. Res.,* **99** (D5), 10 577–10 600.

Stamnes, K., S.-C. Tsay, W. Wiscombe, and I. Laszlo, 1988: A numerically stable algorithm for discrete-ordinate-method radiative transfer in multiple scattering and emitting layered media. *Appl. Opt.,* **27,** 2502–2509.

Stowe, L. L., A. M. Ignatov, and R. R. Singh, 1997: Development, validation and potential enhancement to the second generation operational aerosol product at the National Environmental Satellite, Data and Information Service of the National Oceanic and Atmospheric Administration. *J. Geophys. Res.,* **102** (D14), 16 923–16 934.

——, P. A. Davis, and E. P. McClain, 1999: Scientific basis and initial evaluation of the CLAVR-1 global clear/cloud classification algorithm for the advanced very high resolution radiometer. *J. Atmos. Oceanic Technol.,* **16,** 656–681.

——, H. Jacobowitz, G. Ohring, K. Knapp, and N. Nalli, 2002: The Advanced Very High Resolution Radiometer Pathfinder Atmosphere (PATMOS) Climate Dataset: Initial analyses and evaluations. *J. Climate,* in press.

Tanré, D., Y. J. Kaufman, M. Herman, and S. Mattoo, 1997: Remote sensing of aerosol properties over oceans using the MODIS/EOS spectral radiances. *J. Geophys. Res.,* **102,** 16 971–16 988.

Wang, M., S. Bailey, and C. R. McClain, 2000: SeaWiFS provides unique global aerosol optical property data. *Eos, Trans. Amer. Geophys. Union,* **81,** 197.

Wanner, W., A. H. Strahler, B. Hu, P. Lewis, J.-P. Muller, X. Li, C. L. Barker Schaaf, and M. J. Barnsley, 1997: Global retrieval of bidirectional reflectance and albedo over land from EOS MODIS and MISR data: Theory and algorithm. *J. Geophys. Res.,* **102** (D14), 17 143–17 161.

Zhang, Z., S. N. V. Kalluri, J. Jaja, S. Liang, and J. R. G. Townshend, 1998: Models and high-performance algorithms for global BRDF retrieval. *IEEE Comput. Sci. Eng.*, **5** (4), 16–29.